

Structural, electronic, and spectroscopic effects of Ga-codoping on Ce-doped yttrium aluminum garnet: First-principles study

Ana Belén Muñoz-García¹ and Luis Seijo^{1,2}

¹*Departamento de Química, Universidad Autónoma de Madrid, 28049 Madrid, Spain*

²*Instituto Universitario de Ciencia de Materiales Nicolás Cabrera,
Universidad Autónoma de Madrid, 28049 Madrid, Spain*

(Dated: November 2, 2010)

Abstract

Periodic boundary conditions density-functional theory and embedded cluster wave function theory calculations performed on Ga-doped and Ce,Ga-codoped yttrium aluminum garnet (YAG) $\text{Y}_3\text{Al}_5\text{O}_{12}$, allowed for the determination of the atomistic structures of these materials when Ga substitutes for Al in octahedral and tetrahedral sites and Ce substitutes for Y, as well as for the shifts of the local excited states of main character Ce- $4f^1$, Ce- $5d^1$, and Ce- $6s^1$ induced by Ga-codoping. The experimental blue shift experienced by the lowest Ce $4f \rightarrow 5d$ absorption upon Ga-codoping has been reproduced and it has been found to be caused by the reduction of the effective ligand splitting of the $5d^1$ manifold, which is due to Ga forcing an anisotropic expansion of the surroundings of Ce. The effects of Ga on the energy centroids of the $4f^1$ and $5d^1$ configurations are negligible. The direct electronic effects of Ga are insignificant and all effects of Ga-codoping are a consequence of the geometrical distortions it causes. This picture corresponds to a simple model under use and it contrasts with the case of La-codoping, where the direct electronic effects of La and the centroid energy shift are responsible for the red shift. The reason for such a different behavior could lie in the distance between the dopant and the Ce impurity, which is shorter for Ce,La:YAG than for Ce,Ga:YAG.

PACS numbers: 71.55.Ak, 71.55.-i, 71.15.Dx, 71.15.Qe, 71.15.Nc, 61.72.S-, 61.72.J-, 61.72.-y

I. INTRODUCTION

Controlling the color of white light solid-state lighting devices is considered one of the important issues governing the success of these technologies.¹ Yttrium aluminum garnet $\text{Y}_3\text{Al}_5\text{O}_{12}$, or YAG, doped with Ce^{3+} is a blue-to-yellow downconverter phosphor widely used in white light solid-state lighting devices^{2,3} and its codoping is one of the methods used for its color control⁴⁻⁷ because of the long ago known ability of codopants to act not only as co-activators⁶ but also as wavelength shifters.^{2,8-10} Gd^{3+} and La^{3+} in Ce:YAG shift the yellow luminescence of Ce^{3+} to longer wavelengths (red shift)^{9,10} and Ga^{3+} shifts it to shorter wavelengths (blue shift).^{2,9,10}

Presently, there is an insufficient knowledge on the relationship between the structural changes that codoping induces on the optically active defects, like Ce impurities in Ce:YAG, and the red or blue shifts they produce. This is so mainly because of the difficulties for establishing the detailed local structures of the defects. In the case of codoping Ce:YAG, an empirical rule states tha substitutions of the dodecahedral Y^{3+} by larger ions (like La^{3+}) gives red shift whereas substitutions of the octahedral Al^{3+} by larger ions (like Ga^{3+}) gives blue shift of the Ce^{3+} $5d \rightarrow 4f$ luminescence (and of the first $4f \rightarrow 5d$ absorption),^{4,9,10} although the reasons behind this rule are unknown (the lattice constants increase with both types of substitutions⁹ so that a simple interpretation in terms of changes in the local crystal field around the Ce^{3+} $5d$ shell created by the codopings cannot be made).

In these circumstances, first-principles calculations are expected to be helpful by providing additional insight. In this respect, as a part of a long term first-principles study of the luminescence of Ce in Ce-doped and codoped realistic YAG, which includes the calculation of the luminescence of Ce:YAG (Ref. 11) and the atomistic and electronic structures of perfect YAG (Ref. 12) and of the (always present) single and double antisite defects in YAG (Ref. 13), a study has been recently done on the structural, electronic, and spectroscopic effects on Ce:YAG induced by La-codoping.¹⁴ The calculations of the local structures of Ce_Y single substitutional defect in Ce:YAG and $\text{Ce}_\text{Y}\text{-La}_\text{Y}$ double substitutional defects in Ce,La:YAG and on the lowest $4f \rightarrow 5d$ transitions of Ce:YAG and Ce,La:YAG, revealed a local anisotropic expansion around Ce_Y induced by La-codoping and an associated red shift of the first $4f \rightarrow 5d$ transition.¹⁴ Although the local expansion and the red shift are contradictory on the basis of a simple model that considers only the $5d$ level splitting under the

electric crystal field created by the ligands,⁷ they coexist because the local distortion makes the energy centroid of the $\text{Ce}^{3+}\text{-}5d^1$ configuration to lower significantly and the electronic effects of La, which sits not far from Ce, reduces the ligand field splitting of the $5d$ shell.¹⁴

Here, we present a first-principles study on the effects that Ga-codoping has on the atomistic and electronic structure of Ce:YAG and on the shift of the lowest $4f \rightarrow 5d$ absorption. Under the lack of theoretical and experimental detailed structural data other than the observation of a lattice constant expansion with Ga concentration,⁹ the blue shift experienced by the $5d \rightarrow 4f$ luminescence of Ce:YAG upon Ga-codoping (and of its associated absorption, the first $4f \rightarrow 5d$)^{2,9} has been attributed to a reduction of the splitting of the $5d^1$ levels (larger than that of the $4f^1$ levels), which results from Ga^{3+} lowering the crystal-field around Ce^{3+} as a consequence of Ga-codoping forcing a more cubic environment around Ce^{3+} .^{2,4,8,15} This interpretation assumes that the energy difference between the baricenters of the $4f^1$ and $5d^1$ configurations does not change by Ga-codoping.

We report periodic-boundary-conditions density-functional theory (DFT)^{16,17} calculations of the ground state local structures and electronic structures of $\text{Ga}_{\text{Al}}^{\text{oct}}$ and $\text{Ga}_{\text{Al}}^{\text{tet}}$ single substitutional defects in Ga:YAG at low concentrations ($\text{Y}_3\text{Al}_{2-y}^{\text{oct}}\text{Ga}_y^{\text{oct}}\text{Al}_3^{\text{tet}}\text{O}_{12}$ and $\text{Y}_3\text{Al}_2^{\text{oct}}\text{Al}_{3-y}^{\text{tet}}\text{Ga}_y^{\text{tet}}\text{O}_{12}$ with $y = 0.125$) and of corresponding disubstitutional $\text{Ce}_Y\text{-Ga}_{\text{Al}}^{\text{oct}}$ and $\text{Ce}_Y\text{-Ga}_{\text{Al}}^{\text{tet}}$ defects in the codoped material Ce,Ga:YAG ($\text{Y}_{3-x}\text{Ce}_x\text{Al}_{2-y}^{\text{oct}}\text{Ga}_y^{\text{oct}}\text{Al}_3^{\text{tet}}\text{O}_{12}$ and $\text{Y}_{3-x}\text{Ce}_x\text{Al}_2^{\text{oct}}\text{Al}_{3-y}^{\text{tet}}\text{Ga}_y^{\text{tet}}\text{O}_{12}$ with $x = 0.125$ and $y = 0.125$). [YAG ($\text{Y}_3\text{Al}_5\text{O}_{12}$) belongs to the $Ia\bar{3}d$ (230) space group, it has a 160 atom body-centered cubic unit cell (80 atom primitive cell) with eight formula units of $\text{Y}_3\text{Al}_2^{\text{oct}}\text{Al}_3^{\text{tet}}\text{O}_{12}$, also well described as $\text{Y}_3\text{Al}_2^{\text{oct}}(\text{Al}^{\text{tet}}\text{O}_4)_3$, where the Y atoms occupy 24(c) sites with 8-fold oxygen coordination in a distorted cubic D_2 local symmetry, the Al^{oct} atoms occupy 16(a) sites with 6-fold quasi-octahedral oxygen coordination of S_6 local symmetry, and the Al^{tet} atoms occupy 24(d) sites with 4-fold quasi-tetrahedral oxygen coordination of S_4 local symmetry.]

We also report wave function based calculations (complete-active-space self-consistent-field¹⁸⁻²⁰ based second-order many-body perturbation theory²¹⁻²⁴ calculations, CASSCF/CASPT2) on the ground and excited states of the $(\text{CeO}_8\text{Al}_2\text{O}_4)^{15-}$ cluster embedded in Ga:YAG, using the atomistic structures of Ce,Ga:YAG obtained in the DFT calculations, which, together with the results of the same cluster embedded in YAG (Ref. 14), give the shift of the $4f \rightarrow 5d$ absorption induced by Ga-codoping.

The details of the calculations are presented in Sec. II, the results are discussed and

analyzed in Sec. III and the conclusions presented in Sec. IV.

II. DETAILS OF THE CALCULATIONS

Periodic boundary conditions density functional theory calculations (DFT) and wave function based embedded cluster calculations have been performed in this work. The structures of all defects and their electronic structures have been calculated by means of the self-consistent SIESTA method,^{25,26} using DFT^{16,17} within the generalized gradient approximation (GGA) as formulated by Perdew, Burke, and Ernzerhof^{27,28} (PBE). Norm conserving pseudopotentials²⁹ in the Kleinman-Bylander form³⁰ have been used for all atoms, both in nonrelativistic (Y, Al, O) and relativistic³¹ forms (Ce, Ga). Y, Al, and O pseudopotentials have been taken from Ref. 12, where they were generated for the reference configurations Y($5s^2 4p^6 4d^1$), Al($3s^2 3p^1$), and O($2s^2 2p^4$) and tested in YAG, yttrium aluminum perovskite YAlO₃ (YAP), Al₂O₃, and Y₂O₃. A Ce pseudopotential generated in Ref. 14 for the reference configuration Ce³⁺($5s^2 4p^6 4f^1$) and a Ga pseudopotential generated here for the reference configuration Ga($4s^2 4p^1$) have also been used. Nonlinear partial-core corrections³² have been used for Y, Ce, and Ga, and semicore states for Y and Ce, in order to account for large core-valence overlaps. Atomic basis sets of double- ζ plus polarization quality have been used for all atoms: Y($5s 5s' 4p 4p' 5p 4d 4d'$), Al($3s 3s' 3p 3p' 3d$), O($2s 2s' 2p 2p' 3d$), Ce($5s 6s 6s' 5p 5p' 6p 5d 5d' 4f$), and Ga($4s 4s' 4p 4p' 4d$). The Y, Al, and O basis sets have been taken from Ref. 12 and the Ce basis set from Ref. 14. The Ga basis set has been optimized here by means of the fictitious enthalpy method of Anglada *et al.*³³ in YGaO₃ idealized cubic perovskite with lattice constant 4.04 Å. In order to calculate the exchange-correlation and Hartree matrix elements, the uniform grid in real space on where charge density is projected has been chosen equal to an equivalent plane-wave cutoff converged value of 380 Ry. Total energy calculations have been converged as well with respect to k -space integration; a k grid cutoff of 15.0 Bohr was used.

All geometry optimizations have been performed without imposing any symmetry restrictions in the position of all atoms in the unit cell, using a conjugate gradient method, with a force tolerance of 0.04 eV/Å. Starting geometries were generated from the computed atomistic structure of perfect YAG¹² [$Ia\bar{3}d$ (230) space group, $a=12.114$ Å, $x(\text{O})=-0.036$, $y(\text{O})=0.0519$ and $z(\text{O})=0.1491$, in good agreement with experiment,³⁴] upon substitution of

Y atoms in 24(c) Wyckoff positions with 8-fold D_2 oxygen coordination by Ce and Al atoms in 16(a) positions with 6-fold octahedral oxygen coordination (Al_{oct}) and in 24(d) positions with 4-fold tetrahedral oxygen coordination (Al_{tet}) by Ga, to generate single and double substitutional defects $\text{Ga}_{\text{Al}}^{\text{oct}}$, $\text{Ga}_{\text{Al}}^{\text{tet}}$, $\text{Ce}_Y\text{-Ga}_{\text{Al}}^{\text{oct}}$, and $\text{Ce}_Y\text{-Ga}_{\text{Al}}^{\text{tet}}$. We have explored the change in volume of the unit cell produced by the single substitutional defects by allowing the cell to breathe after optimization of a defect. We obtained lattice constant increments of +0.11% in Ce:YAG and +0.16% in both cases of Ga:YAG, which can be considered negligible, so that all the coordinates and energies in the paper correspond to $a=12.114$ Å.

Thereupon, using relaxed structures obtained according to the method described above, the optical absorption energies corresponding to the $\text{Ce}^{3+} 4f \rightarrow 5d$ transitions in Ce:YAG, Ce, Ga^{oct} :YAG and Ce, Ga^{tet} :YAG have been calculated with embedded cluster wave function based methods. For this purpose, a $(\text{CeO}_8\text{Al}_2\text{O}_4)^{15-}$ embedded cluster was used. The cluster was embedded in *ab initio* model potential (AIMP)³⁵ representations of the pure and Ga-doped hosts YAG and Ga:YAG. The cluster is made of the optically active Ce ion and its first 8-fold oxygen coordination plus two additional AlO_2 atomic sets chosen in such a manner that the two AlO_4 moieties that share two oxygens each with the CeO_8 unit are included in the cluster. These moieties have been shown to be tight and to form strongly bonded -Y- AlO_4 -Y- AlO_4 - chains.¹⁴ The AIMP embedding potentials of Y^{3+} , Al^{3+} , and O^{2-} were taken from Ref. 14, where they were produced for YAG, and the one of Ga^{3+} from Ref. 36, where it was produced in K_2NaGaF_6 . All of them include electrostatic, exchange, and Pauli repulsion interactions between the cluster and its environment.

In the $(\text{CeO}_8\text{Al}_2\text{O}_4)^{15-}$ embedded clusters, spin-orbit free relativistic calculations have been performed using atomistic structures resulting from the previously described ground state periodic boundary conditions DFT calculations. Bonding, static and dynamic correlation, and scalar relativistic effects are taken into account in state-average complete active space self consistent field (SA-CASSCF)¹⁸⁻²⁰ plus multistate second-order perturbation theory (MS-CASPT2)²¹⁻²⁴ calculations performed with a scalar relativistic many-electron Hamiltonian. These calculations are performed with the program MOLCAS.³⁷ Spin-orbit coupling effects are missing in these calculations, but their effect on the $4f \rightarrow 5d$ transitions of Ce:YAG, which are the focus of this paper, are known to be a uniform increment of around 1000 cm^{-1} with negligible dependence on the atomistic structure.¹¹ In the SA-CASSCF calculations, a $[4f, 5d, 6s]^1$ CAS was used, meaning that the wave functions are configuration

interaction (CI) wave functions of all configurations with the unpaired electron occupying one of the thirteen molecular orbitals of main character Ce-4*f*, Ce-5*d*, and Ce-6*s*. The molecular orbitals are chosen so as to minimize the average energy of the thirteen states. No symmetry was used in these calculations. Nevertheless, in Ce:YAG, a local D_2 site is found and the states can be classified as follows: the first seven states result from the splitting of the $4f^1 - {}^2F$ atomic term (1^2A , 1^2B_1 , 2^2B_1 , 1^2B_2 , 2^2B_2 , 1^2B_3 , and 2^2B_3), five states well above result from the splitting of the $5d^1 - {}^2D$ atomic term (2^2A , 3^2A , 3^2B_1 , 3^2B_2 , and 3^2B_3), and a final state is linked to the $6s^1 - {}^2S$ atomic term (4^2A). In Ce,Ga:YAG, the point symmetry is lost and the thirteen states belong to the only irreducible representation of the point group C_1 . They are classified as $1 - 13^2A$, although the relative energies of the $4f^1$, $5d^1$, and $6s^1$ configurations are maintained, as we will see later, and $1 - 7^2A$ are basically of Ce-4*f*¹ character, $8 - 12^2A$ are basically of Ce-5*d*¹ character, and 13^2A of Ce-6*s*¹ character. Using the CASSCF (configuration interaction) wave functions and the (occupied and virtual) molecular orbitals, MS-CASPT2 calculations are done where the dynamic correlation effects (which are missing at the CASSCF level) of the 5*s*, 5*p*, 4*f* and 5*d* electrons of Cerium and the 2*s* and 2*p* electrons of the eight Oxygen atoms are added. In these calculations, a relativistic effective core potential ([Kr] core) and a (14*s*10*p*10*d*8*f*3*g*)/[6*s*5*p*6*d*4*f*1*g*] Gaussian valence basis set from Ref. 38 was used for Ce. For O, a [He] effective core potential and a (5*s*6*p*1*d*)/[3*s*4*p*1*d*] valence basis set from Ref. 39 was used, extended with one p-type diffuse function for anion⁴⁰ and one d-type polarisation function.⁴¹ For Al, we used a [Ne] core potential and a (7*s*6*p*1*d*)/[2*s*3*p*1*d*] valence basis set from Ref. 39, which includes one d-type polarisation function.⁴¹ Extra basis set functions were added in order to improve the degree of orthogonality achieved between the cluster molecular orbitals and the environmental orbitals: the Y³⁺ 3*d*, 4*s*, 4*p* and the Al³⁺ 2*s*, 2*p* atomic orbitals used in the embedding potentials of all Y and Al next to the cluster in Ce:YAG, and the Ga³⁺ 3*s*, 3*p* atomic orbitals in the embedding potentials of the Ga codopant in Ce,Ga:YAG. These type of calculations, as well as embedding potentials, effective core potentials, and basis sets have previously been used in first-principles simulations of Ce:YAG absorption and luminescence¹¹ and of red shift of such transitions upon La-codoping.¹⁴

III. RESULTS AND DISCUSSION

A. $\text{Ga}_{\text{Al}}^{\text{oct}}$ and $\text{Ga}_{\text{Al}}^{\text{tet}}$ single substitutional defects in YAG

1. Structure

In order to study $\text{Ga}_{\text{Al}}^{\text{oct}}$ and $\text{Ga}_{\text{Al}}^{\text{tet}}$ single substitutional defects in YAG, we have performed calculations on the doped materials $\text{Y}_3\text{Al}_{2-y}^{\text{oct}}\text{Ga}_y^{\text{oct}}\text{Al}_3^{\text{tet}}\text{O}_{12}$ and $\text{Y}_3\text{Al}_2^{\text{oct}}\text{Al}_{3-y}^{\text{tet}}\text{Ga}_y^{\text{tet}}\text{O}_{12}$ with $y = 0.125$. For simplicity, we will refer to them as $\text{Ga}_{\text{Al}}^{\text{oct}}\text{:YAG}$ and $\text{Ga}_{\text{Al}}^{\text{tet}}\text{:YAG}$ respectively from now on. They correspond to a Ga_{Al} substitutional defect concentration of 2.5 at.% (one single defect per YAG unit cell).

The formation energies of $\text{Ga}_{\text{Al}}^{\text{oct}}$ and $\text{Ga}_{\text{Al}}^{\text{tet}}$ single substitutional defects at low concentrations according to the processes $8 \text{Y}_3\text{Al}_5\text{O}_{12} + \text{Ga}_{\text{vacuum}}^{3+} \rightarrow 8 \text{Y}_3\text{Al}_{2-y}^{\text{oct}}\text{Ga}_y^{\text{oct}}\text{Al}_3^{\text{tet}}\text{O}_{12} + \text{Al}_{\text{vacuum}}^{3+}$ and $8 \text{Y}_3\text{Al}_5\text{O}_{12} + \text{Ga}_{\text{vacuum}}^{3+} \rightarrow 8 \text{Y}_3\text{Al}_2^{\text{oct}}\text{Al}_{3-y}^{\text{tet}}\text{Ga}_y^{\text{tet}}\text{O}_{12} + \text{Al}_{\text{vacuum}}^{3+}$, with $y = 0.125$, are 1.062 eV/defect (102.5 kJ/mol) and 1.105 eV/defect (106.6 kJ/mol) respectively, which means that substitution in a Al^{oct} site is more favorable than in a Al^{tet} site by 43 meV/defect (4.1 kJ/mol). This quantity changes only to 50 meV/defect when the lattice constant is optimized for each defect. This result means that, at low concentrations, the formation of $\text{Ga}_{\text{Al}}^{\text{oct}}$ defects is only slightly preferred over the formation of $\text{Ga}_{\text{Al}}^{\text{tet}}$ defects. The common assumption is, however, that, at concentrations between 10 and 80 at.%, substitutions at octahedral sites are made before substitutions at tetrahedral sites take place.^{9,10} This assumption is based in part in the fact that Ce luminescence shows a monotonously increasing blue shift between 10 and 40 at.% of Ga_{Al} (40 at.% is the concentration of Al^{oct} sites in YAG), whereas it shows a negligible shift above this concentration and up to 80 at.%.⁹ In this respect, it is interesting to observe that, according to the present calculations, substitution of Al^{oct} in a *rigid*, unrelaxed YAG lattice is more favorable than substitution of Al^{tet} by 633 meV/defect (61 kJ/mol), much more than in a relaxed lattice; however, the tight AlO_4 tetrahedra make the stress energy (the stabilization energy gained by structure relaxation, $E_{\text{stress}} = E_{\text{rigid lattice}} - E_{\text{relaxed lattice}}$) to be larger in Al^{tet} than in Al^{oct} by 590 meV/defect [$E_{\text{stress}}(\text{Ga}_{\text{Al}}^{\text{oct}})=600$ meV/defect, $E_{\text{stress}}(\text{Ga}_{\text{Al}}^{\text{tet}})=1190$ meV/defect], so that it is the lattice relaxation what largely stabilizes Al^{tet} with respect to Al^{oct} making the formation energies of both defects very similar. So, the emerging picture is one in which Ga_{Al} substitutions at octahedral sites are only slightly preferred over substitutions at tetrahedral sites under no

relaxation constraints, although any hindering of relaxation strongly favors the formation of the octahedral substitutional defects. Since increasing defect concentration tends to hinder relaxation, we should expect that $\text{Ga}_{\text{Al}}^{\text{oct}}$ substitutions are dominant over $\text{Ga}_{\text{Al}}^{\text{tet}}$ substitutions at defect concentrations of 10 at.% and above, which are significantly higher than the present one (2.5 at.%), the reason being that octahedral substitutions create much less stress than tetrahedral ones.

Local environments around $\text{Ga}_{\text{Al}}^{\text{oct}}$ and $\text{Ga}_{\text{Al}}^{\text{tet}}$ substitutional defects in $\text{Ga}_{\text{Al}}^{\text{oct}}\text{:YAG}$ and $\text{Ga}_{\text{Al}}^{\text{tet}}\text{:YAG}$ are shown in Fig. 1. Detailed structural data are presented in Table I, which show that Ga produces an homogeneous expansive distortion around it, both in the octahedral and in the tetrahedral sites. This expansion is coherent with the observations of the lattice parameter of $\text{Y}_3\text{Al}_{5-y}\text{Ga}_y\text{O}_{12}$ increasing with Ga concentration from 10 at.% ($y = 0.5$) to 90 at.% ($y = 4.5$).⁹ The breathing is larger in $\text{Ga}_{\text{Al}}^{\text{tet}}$ than in $\text{Ga}_{\text{Al}}^{\text{oct}}$, in consistence with its larger stress energy shown above. The first shell expansions shown here are larger than the ones produced by Ce and La substitution for Y at 8-fold coordination D_2 sites in equivalent calculations.¹⁴ Here, the radial distortions (+0.09 Å in $\text{Ga}_{\text{Al}}^{\text{oct}}$ and +0.14 Å in $\text{Ga}_{\text{Al}}^{\text{tet}}$) are larger than Shannon’s ionic radii mismatches (+0.08 Å in both defects).⁴² Distortions in the second coordination shell are comparable to those in Ce_Y and La_Y defects¹⁴ and, as in those cases, distortions in the third shell are already negligible. This supports the idea that the AlO_4 moieties tightly bonded to Y atoms to form $-\text{Y}-\text{AlO}_4-\text{Y}-\text{AlO}_4-$ chains¹⁴ are flexible enough so as to cushion out distortions in and beyond the third coordination shell.

2. Electronic structure

The band structures of $\text{Ga}_{\text{Al}}^{\text{oct}}\text{:YAG}$ and $\text{Ga}_{\text{Al}}^{\text{tet}}\text{:YAG}$ do not show significant differences from that of pure YAG (Ref. 12) neither in shape nor in dispersion and they are not shown here. Also, the changes in the DOS and PDOS are minimal, as it is illustrated by the corresponding PDOS on Ga and Al shown in Fig. 2. So, even though local geometries are changed upon Ga doping, neither $\text{Ga}_{\text{Al}}^{\text{oct}}$ nor $\text{Ga}_{\text{Al}}^{\text{tet}}$ defects affect the electronic structure of YAG.

B. $\text{Ce}_Y\text{-Ga}_{\text{Al}}^{\text{oct}}$ and $\text{Ce}_Y\text{-Ga}_{\text{Al}}^{\text{tet}}$ double substitutional defects in YAG

1. Structure

In order to study $\text{Ce}_Y\text{-Ga}_{\text{Al}}^{\text{oct}}$ and $\text{Ce}_Y\text{-Ga}_{\text{Al}}^{\text{tet}}$ double substitutional defects in YAG, we have performed calculations on the doubly doped materials $\text{Y}_{3-x}\text{Ce}_x\text{Al}_{2-y}^{\text{oct}}\text{Ga}_y^{\text{oct}}\text{Al}_3^{\text{tet}}\text{O}_{12}$ and $\text{Y}_{3-x}\text{Ce}_x\text{Al}_2^{\text{oct}}\text{Al}_{3-y}^{\text{tet}}\text{Ga}_y^{\text{tet}}\text{O}_{12}$ with $x = 0.125$ and $y = 0.125$. We will call them $\text{Ce}_Y, \text{Ga}_{\text{Al}}^{\text{oct}}\text{:YAG}$ and $\text{Ce}_Y, \text{Ga}_{\text{Al}}^{\text{tet}}\text{:YAG}$ respectively, for simplicity. They correspond to one Ce_Y (4.3 at.%) plus one Ga_{Al} (2.5 at.%) substitutional defects per YAG unit cell, the latter being in an octahedral and in a tetrahedral Al site, respectively. All non-equivalent double defects of each kind have been considered. These are four in $\text{Ce}_Y, \text{Ga}_{\text{Al}}^{\text{oct}}\text{:YAG}$ and seven in $\text{Ce}_Y, \text{Ga}_{\text{Al}}^{\text{tet}}\text{:YAG}$, which are listed in Table II according to their respective Y-Al^{oct} and Y-Al^{tet} distances in perfect YAG. In this Table, the $\text{Ce}_Y\text{-Ga}_{\text{Al}}^{\text{oct}}$ and $\text{Ce}_Y\text{-Ga}_{\text{Al}}^{\text{tet}}$ distances between impurities in the optimized structures are also collected, together with the next distances between impurities and their multiplicity, the relative energies of the double defects, and the interaction energies between single defects, $\Delta E_{\text{sd-inter}}$, defined as the energy difference of the process $8 \text{Y}_{3-x}\text{Ce}_x\text{Al}_5\text{O}_{12} + 8 \text{Y}_3\text{Al}_{5-y}\text{Ga}_y\text{O}_{12} \rightarrow 8 \text{Y}_3\text{Al}_5\text{O}_{12} + 8 \text{Y}_{3-x}\text{Ce}_x\text{Al}_{5-y}\text{Ga}_y\text{O}_{12}$, with $x = 0.125$ and $y = 0.125$.

As we can see in Table II, the most stable double substitutional defects are formed with Ga substituting for Al in the second cation layer around Ce (that is, in its fourth coordination shell), both in octahedral (defect 2, at 5.46 Å) and tetrahedral (defect 7, at 5.66 Å) sites. Their respective formation energies at low concentration according to the processes $8 \text{Y}_3\text{Al}_5\text{O}_{12} + \text{Ce}_{\text{vacuum}}^{3+} + \text{Ga}_{\text{vacuum}}^{3+} \rightarrow 8 \text{Y}_{3-x}\text{Ce}_x\text{Al}_{2-y}^{\text{oct}}\text{Ga}_y^{\text{oct}}\text{Al}_3^{\text{tet}}\text{O}_{12} + \text{Y}_{\text{vacuum}}^{3+} + \text{Al}_{\text{vacuum}}^{3+}$ and $8 \text{Y}_3\text{Al}_5\text{O}_{12} + \text{Ce}_{\text{vacuum}}^{3+} + \text{Ga}_{\text{vacuum}}^{3+} \rightarrow 8 \text{Y}_{3-x}\text{Ce}_x\text{Al}_2^{\text{oct}}\text{Al}_{3-y}^{\text{tet}}\text{Ga}_y^{\text{tet}}\text{O}_{12} + \text{Y}_{\text{vacuum}}^{3+} + \text{Al}_{\text{vacuum}}^{3+}$, with $x = 0.125$ and $y = 0.125$, are 1.137 eV/defect (109.7 kJ/mol) and 1.195 eV/defect (115.3 kJ/mol) respectively. All other defects with impurities at longer distances are slightly more unstable and the instability is largest for the defects with shorter Ce-Ga distances. As shown by the $\Delta E_{\text{sd-inter}}$ values, the single defects attract themselves and tend to get close to each other; however, the local expansions brought about by each of them cannot be accommodated at the same time below a critical distance of around 5.5 Å, under which they repel each other.

As it happens with $\text{Ga}_{\text{Al}}^{\text{oct}}$ and $\text{Ga}_{\text{Al}}^{\text{tet}}$ single defects, in the case of double defects the formation of $\text{Ce}_Y\text{-Ga}_{\text{Al}}^{\text{oct}}$ is only slightly preferred over the formation of $\text{Ce}_Y\text{-Ga}_{\text{Al}}^{\text{tet}}$, by 58 meV/defect

(5.6 kJ/mol). Calculation of their stress energies [$E_{stress}(\text{Ce}_Y\text{-Ga}_{\text{Al}}^{\text{oct}})=760$ meV/defect (73.3 kJ/mol), $E_{stress}(\text{Ce}_Y\text{-Ga}_{\text{Al}}^{\text{tet}})=1334$ meV/defect (128.7 kJ/mol)] reveals that the relaxation of the double defects 2 and 7 is only slightly larger than that of independent single defects [$E_{stress}(\text{Ce}_Y)=125$ meV/defect,¹⁴ $E_{stress}(\text{Ga}_{\text{Al}}^{\text{oct}})=600$ meV/defect, $E_{stress}(\text{Ga}_{\text{Al}}^{\text{tet}})=1190$ meV/defect] by 35 meV/defect (3.4 kJ/mol) and 19 meV/defect (1.8 kJ/mol), respectively, so that the influences of Ce on the different stress energies of the two double defects are minimal. Then, as in the case of single defects, we should expect that stress effects (dominated by Ga_{Al} over Ce_Y) make the formation of $\text{Ce}_Y\text{-Ga}_{\text{Al}}^{\text{oct}}$ double substitutions preferred over the formation of $\text{Ce}_Y\text{-Ga}_{\text{Al}}^{\text{tet}}$ double substitutions at high concentrations.

Local environments around the two most stable double defects $\text{Ce}_Y\text{-Ga}_{\text{Al}}^{\text{oct}}$ (defect 2) and $\text{Ce}_Y\text{-Ga}_{\text{Al}}^{\text{tet}}$ (defect 7) are shown in Fig. 3. Detailed geometrical parameters are presented in Table III. The main effect of Ga-codoping on the local structure around the optically active Ce_Y defect is an overall anisotropic expansion of its first coordination shell, both when Ga substitutes for Al^{oct} and for Al^{tet} ; however, the detailed distortions are very different in both cases: in the former, two of the four closest oxygens move away 0.03 Å and two of the four most distant oxygens approach 0.01 Å, whereas in the latter, one close oxygen moves away 0.07 Å and one distant oxygen approaches 0.01 Å, all other oxygens experiencing shorter displacements. The expansions around Ce_Y supports one of the points of the current interpretation for the Ga-codoping induced blue shift (lowering the crystal-field around Ce), but their high anisotropies do not support at all the other point (forcing a more cubic environment around Ce).^{2,4,8,15} We discuss below the contributions to the blue shift.

2. Electronic structure

The PDOS of Ce, Ga, Y, Al, and O atoms and total DOS of $\text{Ce}_Y\text{Ga}_{\text{Al}}^{\text{oct}}\text{:YAG}$ and $\text{Ce}_Y\text{Ga}_{\text{Al}}^{\text{tet}}\text{:YAG}$ are shown in Fig. 4. They are remarkably similar with the PDOS and DOS of their respective single doped materials $\text{Ga}_{\text{Al}}^{\text{oct}}\text{:YAG}$, $\text{Ga}_{\text{Al}}^{\text{tet}}\text{:YAG}$, and $\text{Ce}_Y\text{:YAG}$, as is the case of the band structures, up to the point that one can safely say that the single defects involved in $\text{Ce}_Y\text{-Ga}_{\text{Al}}^{\text{oct}}$ and $\text{Ce}_Y\text{-Ga}_{\text{Al}}^{\text{tet}}$ are basically independent from the electronic structure point of view.

C. Blue shift of the lowest Ce $4f \rightarrow 5d$ transition upon Ga-codoping

In Table IV we show the transition energies from the ground state to the many-electron states of the configurations Ce- $4f^1$, Ce- $5d^1$, and Ce- $6s^1$, of Ce_Y:YAG, Ce_Y,Ga_{Al}^{oct}:YAG, and Ce_Y,Ga_{Al}^{tet}:YAG. They correspond to MS-CASPT2 calculations on the (CeO₈Al₂O₄)¹⁵⁻ cluster under the effects of AIMP embedding potentials corresponding to YAG (Ref. 14), Ga_{Al}^{oct}:YAG and Ga_{Al}^{tet}:YAG. In Ce_Y:YAG, the states transform according to irreducible representations of the D_2 point group. In Ce_Y,Ga_{Al}^{oct}:YAG, and Ce_Y,Ga_{Al}^{oct}:YAG, the site symmetry around Ce_Y is lost and all the states transform according to the 2A irreducible representation of the C_1 point group; nevertheless, their correspondence with the unperturbed D_2 states of Ce_Y:YAG can be easily established because the energy changes induced by Ga-codoping are small.

The most relevant features in Table IV are the blue shifts experienced by the lowest Ce $4f \rightarrow 5d$ transition [$1^2A(1^2B_2) \rightarrow 8^2A(2^2A)$] upon Ga substitutions for Al^{oct} (74 cm⁻¹) and for Al^{tet} (211 cm⁻¹) at Ga doping concentrations of 2.5 at.%. This result is in qualitative agreement with experiments because blue shifts induced by Ga-codoping have been observed at all doping levels.^{2,4,8,9} Since the formation of Ga_{Al}^{oct} is preferred over Ga_{Al}^{tet}, as discussed above, it is the 74 cm⁻¹ blue shift at 2.5 at.% what corresponds to experiments. Although all of them have been done at higher doping levels, a 50 cm⁻¹ blue shift is deduced from extrapolation of the measurements of Tien *et al.*⁹ at 10 and 20 at.%. The agreement is quite good with some overestimation, as it was the case with the red shift induced by La-codoping.¹⁴

Let us now analyze the reasons behind the blue shift. In order to do so, we will use the diagram in Fig. 5, where the energy levels of Ce_Y,Ga_{Al}^{oct}:YAG are represented together with the centroids of the $4f^1$ and $5d^1$ configurations, $\frac{1}{7} \sum_{i=1,7} E(4f^1 - i^2A)$ and $\frac{1}{5} \sum_{i=1,5} E(5d^1 - (7+i)^2A)$. In the diagram, the transition energy between the lowest levels of the $4f^1$ and $5d^1$ configurations [$1^2A(1^2B_2) \rightarrow 8^2A(2^2A)$] is also indicated, as well as the ligand field stabilization energies of both levels. It is clear that we can write the transition energy in terms of these components as

$$\begin{aligned} \Delta E(4f^1 - 1^2A \rightarrow 5d^1 - 8^2A) &= \Delta E_{\text{centroid}}(4f^1 \rightarrow 5d^1) + \Delta E_{\text{ligand-field}}(1^2A \rightarrow 8^2A) \quad (1) \\ &= \Delta E_{\text{centroid}}(4f^1 \rightarrow 5d^1) + \Delta E_{\text{LF}}(4f^1 - 1^2A) - \Delta E_{\text{LF}}(5d^1 - 8^2A) \quad . \end{aligned}$$

The values of these quantities and their changes upon Ga-codoping are presented in Table IV. They show that the blue shifts induced by $\text{Ga}_{\text{Al}}^{\text{oct}}$ and $\text{Ga}_{\text{Al}}^{\text{tet}}$ are determined by the lowering of the ligand field stabilization energies of the lowest $5d^1$ level, whereas the shift of the energy difference between the $4f^1$ and $5d^1$ centroids upon Ga-codoping is insignificant and it does not play any role in the blue shift. This picture is totally different to the case of the $4f^1 - 1^2A \rightarrow 5d^1 - 8^2A$ shift upon La-codoping,¹⁴ where the relative stabilization of the $5d^1$ centroid dominates the red shift and the increment of the ligand field splitting of the $5d$ shell enhances it, in spite of the fact that both Ga-codoping and La-codoping produce anisotropic expansions around Ce_Y defects. Next, we discuss the reason for this difference.

Table V shows an analysis of the contributions to the shifts experienced by the configuration centroids and the ligand-field stabilization energies due to the first-shell distortion around Ce_Y , the full distortion of the lattice, and the direct electronic effects of Ga. [These effects have been extracted as differences between four MS-CASPT2 calculations on the $(\text{CeO}_8\text{Al}_2\text{O}_4)^{15-}$ embedded cluster: one (A) performed with cluster atomic coordinates, embedding atomic coordinates, and embedding potentials of Ce:YAG, another one (B) with cluster atomic coordinates of Ce,Ga:YAG but embedding atomic coordinates and embedding potentials of Ce:YAG, a third one (C) with cluster and embedding atomic coordinates of Ce,Ga:YAG and embedding potentials of Ce:YAG, and a fourth one (D) with cluster atomic coordinates, embedding atomic coordinates, and embedding potentials of Ce,Ga:YAG, which is the final, real calculation of Ce,Ga:YAG.] Firstly, we observe that there is no significant effect on the centroid energy difference neither by the distortions nor by the direct effects of Ga. In La-codoping,¹⁴ however, both the distortions and the electronic effects of La lower the centroid energy difference to the point of making it the largest contribution to the red shift. The second observation is that the ligand field splittings, which are ultimately responsible for the blue shift upon Ga-codoping, are dominated by the distortions, with the first-shell distortion accounting for approximately two thirds of the whole effect and the remaining distortions for the other third, and the direct effects of Ga are negligible. The effect of the first shell distortion upon La-codoping¹⁴ is the same (lowering $5d$ shell splitting, blue shift) but it is partially compensated by the remaining distortions which act in the opposite direction, and, most importantly, the direct electronic effects of La are relevant and increase the $5d$ shell splitting, so given another important contribution to the red shift. As a conclusion of this analysis we can say that the effects of Ga-codoping on the blue shift

of the lowest $\text{Ce}^{3+} 4f \rightarrow 5d$ transition of $\text{Ce}:\text{YAG}$ can be described with a simple model in which Ga acts only by provoking an expansion around Ce_Y , whose main effect is lowering the $5d$ shell splitting.^{4,9,10} However, this model cannot be applied to the red shift induced by La-codoping, where the direct electronic effects of La and the centroid energy shift are instrumental.¹⁴ The reason for such a different behavior could lie in the distance between the dopant and the Ce impurity, which is shorter in $\text{Ce}_Y\text{-La}_Y$ (3.73 \AA)¹⁴ than in $\text{Ce}_Y\text{-Ga}_{\text{Al}}^{\text{oct}}$ (5.46 \AA) and $\text{Ce}_Y\text{-Ga}_{\text{Al}}^{\text{tet}}$ (5.66 \AA).

IV. CONCLUSIONS

A combined (PBC DFT and embedded cluster MS-CASPT2) first-principles study has been made on $\text{Ga}:\text{YAG}$ and $\text{Ce,Ga}:\text{YAG}$ which provides the atomistic structures of the doped and co-doped materials and the energy shifts of the excited states of $\text{Ce}:\text{YAG}$ with main character $\text{Ce-}4f^1$, $\text{Ce-}5d^1$, and $\text{Ce-}6s^1$ induced by Ga-codoping. The experimental Ga-induced $\text{Ce } 4f \rightarrow 5d$ blue shift has been reproduced; its analysis reveals that it is due to a reduction of the effective ligand splitting of the $5d^1$ manifold together with a null effect on the centroids of the $4f^1$ and $5d^1$ configurations. The direct electronic effects of Ga on these properties are negligible, so that all the effects of Ga-codoping are basically the consequence of the geometrical distortions around Ce it causes. These behaviors are opposite to the case of La-codoping, where the direct electronic effects of La and the centroid energy shift are responsible for the red observed shift.¹⁴ The reason for such a different behavior could lie in the distance between the dopant and the Ce impurity, which is shorter in $\text{Ce}_Y\text{-La}_Y$ than in $\text{Ce}_Y\text{-Ga}_{\text{Al}}^{\text{oct}}$ and $\text{Ce}_Y\text{-Ga}_{\text{Al}}^{\text{tet}}$.

Acknowledgments

This work was partly supported by a grant from Ministerio de Ciencia e Innovación, Spain (Dirección General de Programas y Transferencia de Conocimiento MAT2008-05379/MAT). A.B.M.-G. acknowledges a contract of the program Personal Investigador de Apoyo (PIA,

Comunidad de Madrid).

- ¹ J. Brodrick, J. Disp. Technol. **3**, 91 (2007).
- ² G. Blasse and A. Bril, J. Chem. Phys. **47**, 5139 (1967).
- ³ T. Jüstel, H. Nikol, and C. Ronda, Angew. Chem., Int. Ed. **37**, 3084 (1998).
- ⁴ Y. Pan, M. Wu, and Q. Su, J. Phys. Chem. Solids **65**, 845 (2004).
- ⁵ Y. S. Lin, R. S. Liu, and B.-M. Cheng, J. Electrochem. Soc. **152**, J41 (2005).
- ⁶ H. S. Jang, W. B. Im, D. C. Lee, D. Y. Jeon, and S. S. Kim, J. Lumin. **126**, 371 (2007).
- ⁷ Y. X. Pan, W. Wang, G. K. Liu, S. Skanthakumar, R. A. Rosenberg, X. Z. Guo, and K. K. Li, J. Alloys Compd. **488**, 638 (2009).
- ⁸ W. W. Holloway and M. Kestigian, J. Opt. Soc. Am. **59**, 60 (1969).
- ⁹ T. Y. Tien, E. F. Gibbons, R. G. DeLosh, P. J. Zacmanidis, D. E. Smith, and H. L. Stadler, J. Electrochem. Soc. **120**, 278 (1973).
- ¹⁰ J. M. Robertson, M. W. van Tol, W. H. Smits, and J. P. H. Heynen, Philips J. Res. **36**, 15 (1981).
- ¹¹ J. Gracia, L. Seijo, Z. Barandiarán, D. Curulla, H. Niemansverdriet, and W. van Gennip, J. Lumin. **128**, 1248 (2008).
- ¹² A. B. Muñoz-García, E. Anglada, and L. Seijo, Int. J. Quantum Chem. **109**, 1991 (2009).
- ¹³ A. B. Muñoz-García, E. Artacho, and L. Seijo, Phys. Rev. B **80**, 014105 (2009).
- ¹⁴ A. B. Muñoz-García, J. L. Pascual, Z. Barandiarán, and L. Seijo, Phys. Rev. B **82**, 064114 (2010).
- ¹⁵ P. N. Hooge, J. Chem. Phys. **45**, 4504 (1966).
- ¹⁶ P. Hohenberg and W. Kohn, Phys. Rev. B **136**, B864 (1964).
- ¹⁷ W. Kohn and L. J. Sham, Phys. Rev. **140**, A1133 (1965).
- ¹⁸ B. O. Roos, P. R. Taylor, and P. E. M. Siegbahn, Chem. Phys. **48**, 157 (1980).
- ¹⁹ P. E. M. Siegbahn, A. Heiberg, B. O. Roos, and B. Levy, Phys. Scr. **21**, 323 (1980).
- ²⁰ P. E. M. Siegbahn, A. Heiberg, J. Almlöf, and B. O. Roos, J. Chem. Phys. **74**, 2384 (1981).
- ²¹ K. Andersson, P.-Å. Malmqvist, B. O. Roos, A. J. Sadlej, and K. Wolinski, J. Phys. Chem. **94**, 5483 (1990).
- ²² K. Andersson, P.-Å. Malmqvist and B. O. Roos, J. Chem. Phys. **96**, 1218 (1992).

- ²³ A. Zaitsevskii and J. P. Malrieu, Chem. Phys. Lett. **233**, 597 (1995).
- ²⁴ J. Finley, P.-Å. Malmqvist, B. O. Roos and L. Serrano-Andrés, Chem. Phys. Lett. **288**, 299 (1998).
- ²⁵ P. Ordejón, E. Artacho, and J. M. Soler, Phys. Rev. B **53**, R10441 (1996).
- ²⁶ J. M. Soler, E. Artacho, J. D. Gale, A. García, J. Junquera, P. Ordejón, and D. Sánchez-Portal, J. Phys.: Condens. Matter **14**, 2745 (2002).
- ²⁷ J. P. Perdew, K. Burke, and M. Ernzerhof, Phys. Rev. Lett. **77**, 3865 (1996).
- ²⁸ J. P. Perdew, K. Burke, and M. Ernzerhof, Phys. Rev. Lett. **78**, 1396 (1997).
- ²⁹ N. Troullier and J. L. Martins, Phys. Rev. B **43**, 1993 (1991).
- ³⁰ L. Kleinman and D. M. Bylander, Phys. Rev. Lett. **48**, 1425 (1982).
- ³¹ G. B. Bachelet, D. R. Hamann, and M. Schlüter, Phys. Rev. B **26**, 4199 (1982).
- ³² S. G. Louie, S. Froyen, and M. Cohen, Phys. Rev. B **26**, 1738 (1982).
- ³³ E. Anglada, J. M. Soler, J. Junquera, and E. Artacho, Phys. Rev. B **66**, 205101 (2002).
- ³⁴ F. Euler and J. A. Bruce, Acta Crystallogr. **19**, 971 (1965).
- ³⁵ Z. Barandiarán and L. Seijo, J. Chem. Phys. **89**, 5739 (1988).
- ³⁶ Z. Barandiarán, L. Seijo, and L. G. M. Pettersson, J. Chem. Phys. **98**, 4041 (1993).
- ³⁷ G. Karlström, R. Lindh, P. A. Malmqvist, B. O. Roos, U. Ryde, V. Veryazov, P. O. Widmark, M. Cossi, B. Schimmelpfennig, P. Neogady, and L. Seijo, Comput. Mater. Sci. **28**, 222 (2003).
- ³⁸ L. Seijo, Z. Barandiarán, and B. Ordejón, Mol. Phys. **101**, 73 (2003).
- ³⁹ Z. Barandiarán and L. Seijo, Can. J. Chem. **70**, 409 (1992).
- ⁴⁰ T. H. Dunning and P. J. Hay, in *Modern Theoretical Chemistry*, edited by H. F. Schaefer III (Plenum, New York, 1977).
- ⁴¹ J. Andzelm, M. Klobukowski, E. Radzio-Andzelm, Y. Sakai, and H. Tatewaki, *Gaussian Basis Sets for Molecular Calculations*, edited by S. Huzinaga, (Elsevier, Amsterdam, 1984).
- ⁴² R. D. Shannon, Acta Crystallogr. A **32**, 751 (1976).

TABLE I: Distortions in the first and second coordination shells around $\text{Ga}_{\text{Al}}^{\text{oct}}$ and $\text{Ga}_{\text{Al}}^{\text{tet}}$ single substitutional defects with respect to pure YAG. For each atom, $d(\text{M-atom})$, δr_{\parallel} , δr_{\perp} , and Θ are given, which stand, respectively, for its distance to M, the radial and perpendicular displacements along the M-atom axis, and the angle between the radial displacement and the displacement vector of the atom. α stands for angles between three atoms. Atom labels correspond to Fig. 1. Distances in Å, angles in degree.

		YAG, M=Al	Ga:YAG, M=Ga
$\text{Ga}_{\text{Al}}^{\text{oct}}$ substitutional defect			
M-O	$d(\text{M-O})$	1.948	2.039(+4.7%)
	δr_{\parallel}	-	0.091
	δr_{\perp}	-	0.022
	Θ	-	13.7
$\alpha(\text{Oa-B-Ob})$		93.5	94.0
$\alpha(\text{Ob-B-Oc})$		86.5	85.1
$\alpha(\text{Oa-B-Oc})$		180.0	180.0
M-Al ^{tet}	$d(\text{M-Al}^{\text{tet}})$	3.386	3.424(+1.1%)
	δr_{\parallel}	-	0.039
	δr_{\perp}	-	0.011
	Θ	-	16.5
M-Y	$d(\text{M-Y})$	3.386	3.407(+0.6%)
	δr_{\parallel}	-	0.021
	δr_{\perp}	-	0.008
	Θ	-	20.5
$\text{Ga}_{\text{Al}}^{\text{tet}}$ substitutional defect			
M-O	$d(\text{M-O})$	1.788	1.924(+7.6%)
	δr_{\parallel}	-	0.135
	δr_{\perp}	-	0.036
	Θ	-	15.0
$\alpha(\text{Oa-T-Ob})$		100.5	100.3
$\alpha(\text{Oa-T-Oc})$		114.2	114.2
$\alpha(\text{Oa-T-Od})$		114.2	114.2
$\alpha(\text{Ob-T-Oc})$		114.2	114.2
$\alpha(\text{Ob-T-Od})$		114.2	114.2
$\alpha(\text{Oc-T-Od})$		100.5	100.3
M-Al ^{oct}	$d(\text{M-Al}^{\text{oct}})$	3.386	3.416(+0.9%)
	δr_{\parallel}	-	0.030
	δr_{\perp}	-	0.002
	Θ	-	3.5
M-Y1	$d(\text{M-Y1})$	3.028	3.047(+0.6%)
	δr_{\parallel}	-	0.018
	δr_{\perp}	-	~ 0
	Θ	-	~ 0
M-Y2	$d(\text{M-Y1})$	3.709	3.726(+0.5%)
	δr_{\parallel}	-	0.017
	δr_{\perp}	-	0.004
	Θ	-	13.3

TABLE II: Distances between impurities in the $\text{Ce}_Y\text{-Ga}_{\text{Al}}^{\text{oct}}$ and $\text{Ce}_Y\text{-Ga}_{\text{Al}}^{\text{tet}}$ double substitutional defects [$d(\text{Ce}_Y\text{-Ga}_{\text{Al}}^{\text{oct}})$ and $d(\text{Ce}_Y\text{-Ga}_{\text{Al}}^{\text{tet}})$] as compared with Y-Al distances in undoped YAG [$d(\text{Y-Al}^{\text{oct}})$ and $d(\text{Y-Al}^{\text{tet}})$]; values in Å, shifts are shown in parenthesis. The values of the shortest distances between impurities in different unit cells are also given, together with their multiplicity. Relative defect energies with respect to the most stable one (ΔE_{rel}) and interaction energies between single defects ($\Delta E_{\text{sd-inter}}$), in meV/defect and kJ/mol (in parenthesis).

CeY-Ga _{Al} ^{oct} double substitutional defects					
	$d(\text{Y-Al}^{\text{oct}})$	$d(\text{Ce}_Y\text{-Ga}_{\text{Al}}^{\text{oct}})$ intra-cell	$d(\text{Ce}_Y\text{-Ga}_{\text{Al}}^{\text{oct}})$ inter-cell	ΔE_{rel}	$\Delta E_{\text{sd-inter}}^a$
defect 1	3.386	3.436 (+0.050)	9.165 x 1	154 (14.8)	116 (11.1)
defect 2	5.459	5.456 (-0.003)	8.156 x 1	0 (0) ^b	-38 (-3.7)
defect 3	6.938	6.938 (0.000)	6.955 x 1	17 (1.6)	-21 (-2.1)
defect 4	8.155	8.155 (0.000)	8.155 x 1	39 (3.8)	1 (0.1)
CeY-Ga _{Al} ^{tet} double substitutional defects					
	$d(\text{Y-Al}^{\text{tet}})$	$d(\text{Ce}_Y\text{-Ga}_{\text{Al}}^{\text{tet}})$ intra-cell	$d(\text{Ce}_Y\text{-Ga}_{\text{Al}}^{\text{tet}})$ inter-cell		
defect 5	3.028	3.056 (+0.028)	9.059 x 1	255 (24.6)	174 (16.8)
defect 6	3.709	3.755 (+0.046)	9.312 x 1	281 (27.1)	200 (19.3)
defect 7	5.666	5.655 (-0.011)	8.294 x 1	58 (5.6)	-23 (-2.2)
defect 8	6.057	6.056 (-0.001)	6.058 x 1	86 (8.3)	5 (0.5)
defect 9	7.103	7.104 (+0.001)	9.331 x 1, 9.337 x 1	83 (8.0)	2 (0.2)
defect 10	8.566	8.562 (-0.004)	8.565 x 1, 8.567 x 1, 8.569 x 1	86 (8.3)	5 (0.5)
defect 11	9.085	9.087 (+0.002)	9.085 x 1, 9.087 x 1, 9.089 x 1	84 (8.1)	3 (0.3)

^a $\Delta E_{\text{sd-inter}} = 8 [\text{E}(\text{Y}_3\text{Al}_5\text{O}_{12}) + \text{E}(\text{Y}_{3-x}\text{Ce}_x\text{Al}_{5-y}\text{Ga}_y\text{O}_{12}) - \text{E}(\text{Y}_{3-x}\text{Ce}_x\text{Al}_5\text{O}_{12}) - \text{E}(\text{Y}_3\text{Al}_{5-y}\text{Ga}_y\text{O}_{12})]$, with $x = 0.125$ and $y = 0.125$

^bFormation energy of this defect from the ions *in vacuo* is 1.137 eV/defect (115.3 kJ/mol); see text for details.

TABLE III: Selected interatomic distances in the most stable $\text{CeY-Ga}_{\text{Al}}^{\text{oct}}$ and $\text{CeY-Ga}_{\text{Al}}^{\text{tet}}$ double substitutional defects in Ce,Ga:YAG , in Å. Reference distances in Ce:YAG and Ga:YAG are also given. Atomic labels correspond to Fig. 3. Type 1 and type 2 oxygen atoms refer to those in the 8-fold coordination shell of Ce which are, respectively, closer and more distant to it. Changes with respect to the respective single substitutional defects CeY , $\text{Ga}_{\text{Al}}^{\text{oct}}$, and $\text{Ga}_{\text{Al}}^{\text{tet}}$ are given in parentheses.

YAG	$d(\text{Y-Al}^{\text{oct}})$	5.459	$d(\text{Y-Al}^{\text{tet}})$	5.666
Ce:YAG	$d(\text{CeY-Al}^{\text{oct}})$	5.461	$d(\text{CeY-Al}^{\text{tet}})$	5.667
Ga:YAG	$d(\text{Y-Ga}_{\text{Al}}^{\text{oct}})$	5.461	$d(\text{Y-Ga}_{\text{Al}}^{\text{tet}})$	5.668
Ce,Ga:YAG	$\text{CeY-Ga}_{\text{Al}}^{\text{oct}}:\text{YAG}$ (defect 2)		$\text{CeY-Ga}_{\text{Al}}^{\text{tet}}:\text{YAG}$ (defect 7)	
	$d(\text{CeY-Ga}_{\text{Al}}^{\text{oct}})$	5.456	$d(\text{CeY-Ga}_{\text{Al}}^{\text{tet}})$	5.655
CeO ₈ moiety				
Oxygens of type 1				
	$d(\text{CeY-O}_1)$	2.406 (+0.033)	$d(\text{CeY-O}_1)$	2.367 (−0.006)
	$d(\text{CeY-O}_2)$	2.371 (−0.002)	$d(\text{CeY-O}_2)$	2.368 (−0.005)
	$d(\text{CeY-O}_5)$	2.373 (0.000)	$d(\text{CeY-O}_5)$	2.440 (+0.067)
	$d(\text{CeY-O}_6)$	2.407 (+0.034)	$d(\text{CeY-O}_6)$	2.370 (−0.003)
Oxygens of type 2				
	$d(\text{CeY-O}_3)$	2.473 (+0.005)	$d(\text{CeY-O}_3)$	2.454 (−0.014)
	$d(\text{CeY-O}_4)$	2.471 (+0.003)	$d(\text{CeY-O}_4)$	2.470 (+0.002)
	$d(\text{CeY-O}_7)$	2.454 (−0.014)	$d(\text{CeY-O}_7)$	2.461 (−0.007)
	$d(\text{CeY-O}_8)$	2.456 (−0.012)	$d(\text{CeY-O}_8)$	2.472 (+0.004)
GaO ₆ moiety				
	$d(\text{Ga}_{\text{Al}}^{\text{oct}}-\text{O}_a)$	2.053 (+0.014)	GaO ₄ moiety	
	$d(\text{Ga}_{\text{Al}}^{\text{oct}}-\text{O}_b)$	2.040 (+0.001)		
	$d(\text{Ga}_{\text{Al}}^{\text{oct}}-\text{O}_c)$	1.962 (−0.077)		
	$d(\text{Ga}_{\text{Al}}^{\text{oct}}-\text{O}_d)$	2.043 (+0.004)		
	$d(\text{Ga}_{\text{Al}}^{\text{oct}}-\text{O}_e)$	2.054 (+0.015)		
	$d(\text{Ga}_{\text{Al}}^{\text{oct}}-\text{O}_f)$	2.040 (+0.001)		
	$d(\text{Ga}_{\text{Al}}^{\text{tet}}-\text{O}_a)$	1.924 (0.000)	GaO ₄ moiety	
	$d(\text{Ga}_{\text{Al}}^{\text{tet}}-\text{O}_b)$	1.921 (−0.003)		
	$d(\text{Ga}_{\text{Al}}^{\text{tet}}-\text{O}_c)$	1.928 (+0.004)		
	$d(\text{Ga}_{\text{Al}}^{\text{tet}}-\text{O}_d)$	1.926 (+0.002)		

TABLE IV: Relative energies of the many-electron levels of the Ce- $4f^1$, Ce- $5d^1$, and Ce- $6s^1$ configurations in Ce_Y:YAG, Ce_Y,Ga_{Al}^{oct}:YAG, and Ga_{Al}^{tet}:YAG, and shifts induced by Ga-codoping Ce:YAG. MS-CASPT2 calculations on the (CeO₈Al₂O₄)¹⁵⁻ embedded cluster. All numbers in cm⁻¹.

	Ce _Y :YAG ^a		C_1 point group	Ce _Y ,Ga _{Al} ^{oct} :YAG		Ce _Y ,Ga _{Al} ^{tet} :YAG	
	D_2 point group	Energy		Energy	Shift	Energy	Shift
$4f^1$ levels							
	1^2B_2	0	1^2A	0		0	
	1^2B_3	38	2^2A	51	13	64	26
	1^2B_1	202	3^2A	244	42	231	29
	1^2A	416	4^2A	421	5	409	-7
	2^2B_1	443	5^2A	473	30	445	2
	2^2B_2	516	6^2A	524	8	529	13
	2^2B_3	2419	7^2A	2420	1	2390	-29
$5d^1$ levels							
	2^2A	23853	8^2A	23927	74	24064	211
	3^2B_3	30169	9^2A	30247	76	30278	109
	3^2A	48112	10^2A	48328	216	47884	-228
	3^2B_2	48700	11^2A	49080	380	48990	290
	3^2B_1	52221	12^2A	51555	-666	51719	-502
$6s^1$ level							
	4^2A	61214	13^2A	61957	743	61627	413
$\Delta E_{\text{centroid}}(4f^1 \rightarrow 5d^1)$		40035		40037	2	40006	-29
$\Delta E_{\text{ligand-field}}(1^2A \rightarrow 8^2A)$		-16182		-16110	72	-15942	240
$\Delta E_{\text{LF}}(4f^1 - 1^2A)$		576		591	15	581	5
$\Delta E_{\text{LF}}(5d^1 - 8^2A)$		16758		16701	-57	16523	-235

^aReference 14

TABLE V: Analysis of contributions to the shift of the lowest $4f \rightarrow 5d$ transition [$1^2A(1^2B_2) \rightarrow 8^2A(2^2A)$] from Ce:YAG to Ce,Ga:YAG. All numbers in cm^{-1} .

	First-shell distortion	Contributions Full distortion	Ga	All
	Ce _Y ,Ga _{Al} ^{oct} :YAG			
$\Delta E(4f^1 - 1^2A \rightarrow 5d^1 - 8^2A)$	52	78	-4	74
$\Delta E_{\text{centroid}}(4f^1 \rightarrow 5d^1)$	-3	2	0	2
$\Delta E_{\text{ligand-field}}$	55	76	-4	72
$\Delta E_{\text{LF}}(4f^1 - 1^2A)$	13	18	-3	15
$\Delta E_{\text{LF}}(5d^1 - 8^2A)$	-42	-57	0	-57
	Ce _Y ,Ga _{Al} ^{tet} :YAG			
$\Delta E(4f^1 - 1^2A \rightarrow 5d^1 - 8^2A)$	125	211	0	211
$\Delta E_{\text{centroid}}(4f^1 \rightarrow 5d^1)$	-27	-30	1	-29
$\Delta E_{\text{ligand-field}}$	152	241	-1	240
$\Delta E_{\text{LF}}(4f^1 - 1^2A)$	21	5	0	5
$\Delta E_{\text{LF}}(5d^1 - 8^2A)$	-131	-236	1	-235

FIG. 1: First and second coordination shells around a $\text{Ga}_{\text{Al}}^{\text{oct}}$ defect (above) and a $\text{Ga}_{\text{Al}}^{\text{tet}}$ defect (below) in YAG. Oxygen labels correspond to Table I. Above: $\text{Ga}_{\text{Al}}^{\text{oct}}$ is labelled B; three of the six symmetry equivalent oxygens in the first coordination shell are labelled; the second shell is made of six equivalent Al^{tet} atoms and six equivalent Y atoms. Below: $\text{Ga}_{\text{Al}}^{\text{tet}}$ is labelled T; the four symmetry equivalent oxygens in the first coordination shell are labelled; the second shell is made of four equivalent Al^{oct} atoms and two sets of equivalent Y atoms, labelled Y1 (two) and Y2 (four).

FIG. 2: PDOS of Ga, Al, Y, and O atoms and DOS of $\text{Ga}_{\text{Al}}^{\text{oct}}:\text{YAG}$ (above) and $\text{Ga}_{\text{Al}}^{\text{tet}}:\text{YAG}$ (below). PDOS of substituted Al^{oct} and Al^{tet} individual atoms for pure YAG are also shown for comparison.

FIG. 3: Representation of the most stable $\text{Ce}_Y\text{-Ga}_{\text{Al}}^{\text{oct}}$ (above) and $\text{Ce}_Y\text{-Ga}_{\text{Al}}^{\text{tet}}$ (below) double substitutional defects. Atom labels correspond to Table III.

FIG. 4: PDOS of Ce, Ga, Al, Y and O atoms and DOS of $\text{Ce,Ga}_{\text{Al}}^{\text{oct}}:\text{YAG}$ (above) and $\text{Ce,Ga}_{\text{Al}}^{\text{tet}}:\text{YAG}$ (below).

FIG. 5: $4f^1$ and $5d^1$ energy levels of $\text{Ce}_Y\text{,Ga}_{\text{Al}}^{\text{oct}}:\text{YAG}$ as calculated in this work. The energy of the lowest $4f \rightarrow 5d$ transition is indicated together with the energy difference between the centroids of the $4f^1$ and $5d^1$ configurations, $\Delta E_{\text{centroid}}$, and the ligand-field stabilization energies of the lowest states of each configuration, ΔE_{LF} .

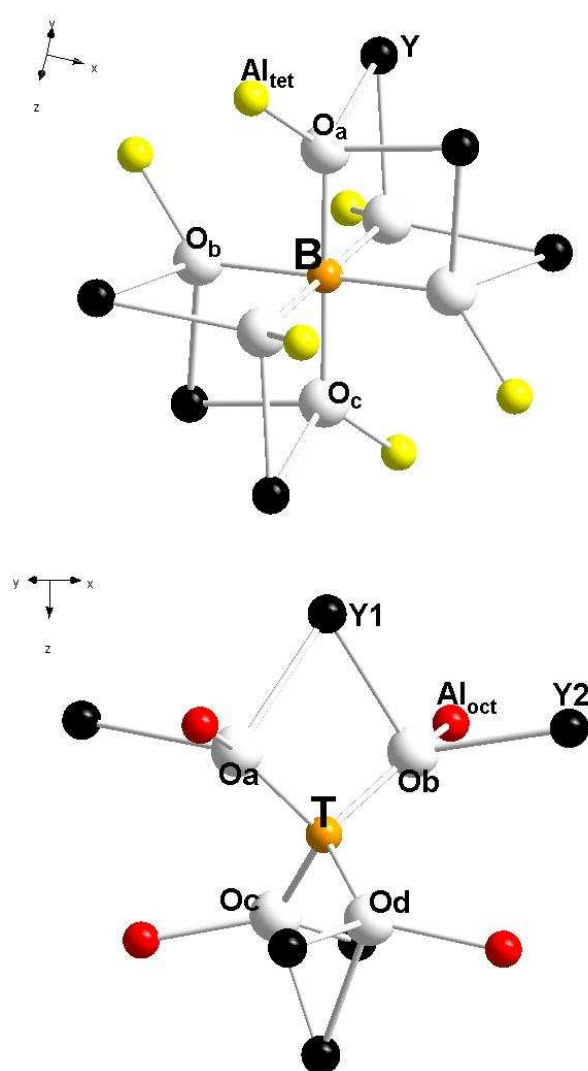


Figure 1 Muñoz-García and Seijo

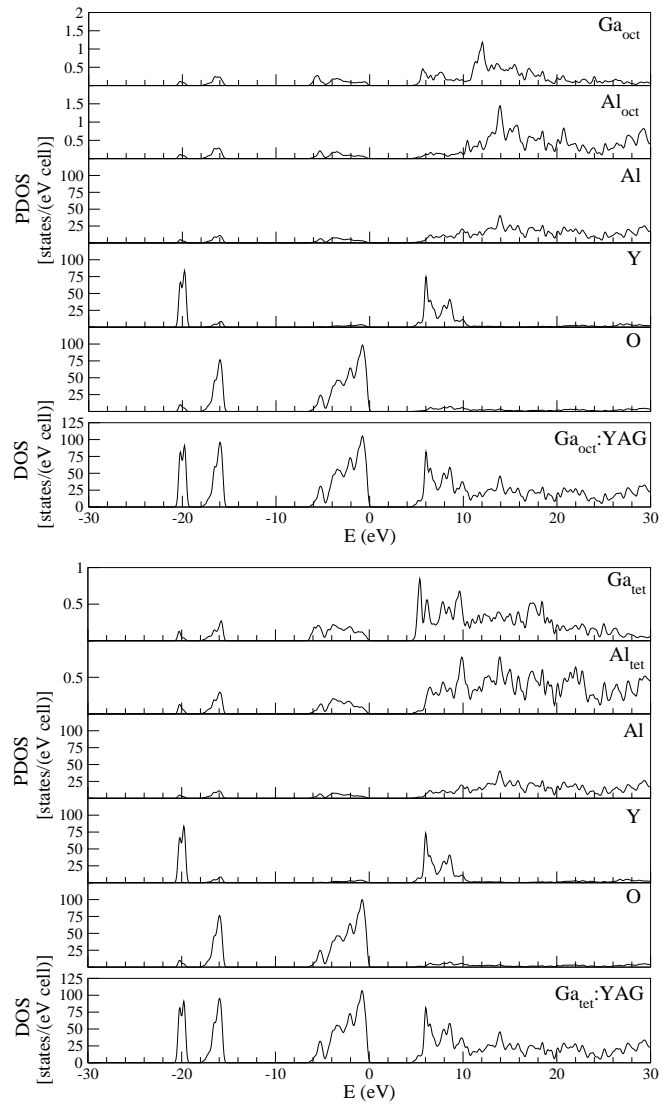


Figure 2 Muñoz-García and Seijo

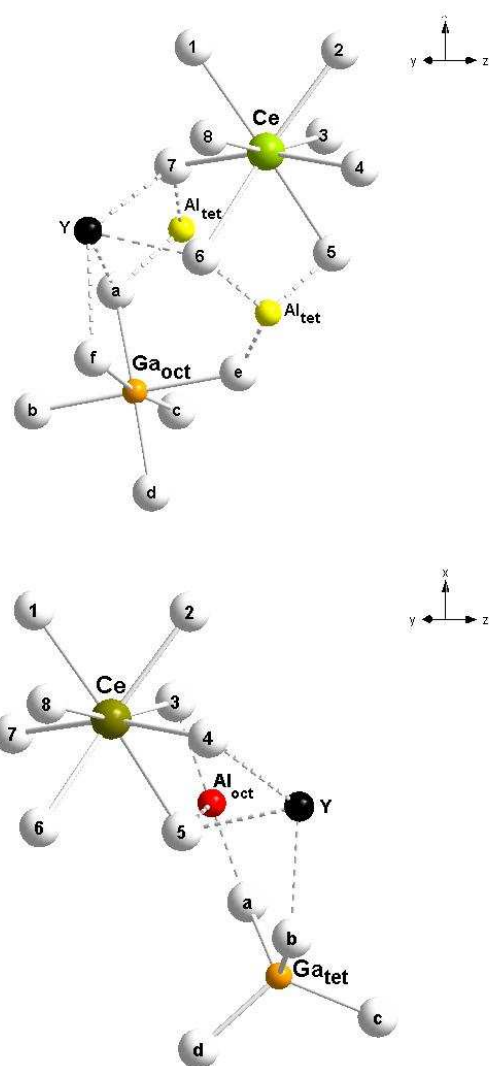


Figure 3 Muñoz-García and Seijo

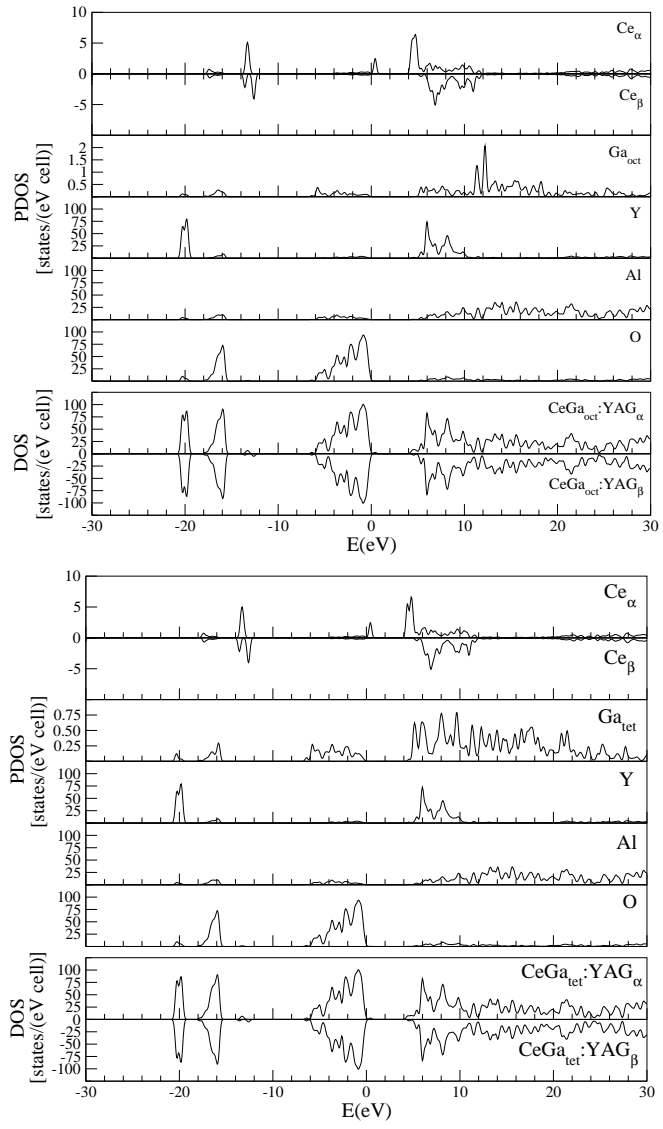


Figure 4 Muñoz-García and Seijo

Figure 5 Muñoz-García and Seijo

